The Engineering Society For Advancing Mobility Land Sea Air and Space®

400 COMMONWEALTH DRIVE WARRENDALE, PA 15096

SAE Technical Paper Series

872110

Autoignition of Adiabatically Compressed Combustible Gas Mixtures

Haoran Hu and James Keck
Massachusetts Institute of Technology

International Fuels and Lubricants Meeting and Exposition
Toronto, Ontario
November 2-5, 1987

872110

Autoignition of Adiabatically Compressed Combustible Gas Mixtures

Haoran Hu and James Keck
Massachusetts Institute of Technology

ABSTRACT

Measurements of explosion limits for fuel/air/diluent mixtures compressed by an expanding laminar flame have been made in a constant volume spherical bomb. The fuels studied to date range from butane to octane at fuel/air equivalence ratios from 0.8 to 1.3. The explosion pressures and temperatures range from 10 to 100 atm and 650 to 850 K. The pressure versus time curves show the behavior typical of the two-stage ignition process observed in rapid compression machines.

A branched chain kinetic model has been developed to correlate the data. The model has been used to predict both the explosion limits measured in the current bomb experiments and ignition delays measured in prior rapid compression machine experiments. Good agreement between experiment and theory can be achieved with minor adjustment in published rate constants.

AUTOIGNITION OF ADIABATICALLY compressed combustible charges is one of the most basic combustion processes, and determining the chemical kinetic mechanism involved has been a major goal of combustion research for the past half century[1,2]. An understanding of this combustion process is important for the study of knock in spark ignition engines and autoignition in diesel engines[3,4].

Autoignition is the onset of combustion in a reactive charge without the introduction of an external igniting source. It has been observed to be either a single- or two-stage event depending on the physical conditions and the fuel[5,6]. It is now widely accepted that engine knock is a result of autoignition of the unburned portion of the fuel-air charge as it is compressed and heated adiabatically by the motion of the piston and by the expansion of burned gas behind the advancing flame front[3,4].

Because of the physical complexities of the internal combustion engine, many experimental investigations of knock have been made by isolating the autoignition process and studying it in simpler physical environment[1,5,6,7,8]. However the explosion limits, the limits of the region of temperature and pressure for which autoignition occurs, have not previously been satisfactorily correlated, and data obtained in rapid compression machines operating under similar conditions disagree[5,6].

Products analysis studies[4] reveal an enormous number of intermediate products in the combustion of hydrocarbons of only moderate molecular mass. This indicates that the kinetics of the chemical reaction leading up to autoignition are complex even for simple pure hydrocarbon fuels. Fundamental theoretical studies of hydrocarbon combustion have involved the cataloging of a large number of chemical reactions that may occur between the fuel and air and many intermediate species. The resulting set of up to several hundred reaction rate equations must then be integrated numerically. Pitz and Westbrook[9] have summarized the combustion of butane and air for hundreds of species and rate equations. The solution of such large sets of equations is difficult and may yield little insight into the rate limiting reactions in the process. Therefore, many researchers have limited their studies to a few key rate limiting kinetic reactions in describing the process leading to autoignition.

An important investigation conducted by the Shell-Thornton Research Center[10], has focused on a description of the chemical system which contains three generalized intermediates, obtaining a governing set of six differential equations. With suitably chosen parameters, the model is able to simulate the two stage phenomena of high-pressure autoignition. Cox and Cole[11] have refined the Shell model by providing kinetic information on elementary hydrocarbon reaction processes. The Shell model

* Numbers in brackets designate references at end of paper.

0148-7191/87/1102-2110$02.50

has been applied to engine autoignition studies by several investigators[12], and recently Theobald[13] has used the Shell model for diesel engine autoignition simulation. However, in order to achieve good agreement with experimental results, certain parameters in the Shell model are required to take values different from those expected from the original hydrocarbon oxidation mechanism on which the model was based. In addition, kinetic models used by different authors vary considerably [10,11,14,15] and the rate constants for hydrocarbon fuels with more than one carbon atom are based largely on estimates[11,15,16]. Thus there is a need for further experimental studies carried out under controlled conditions as well as further kinetic modeling.

In response to these needs, this paper is concerned with both experimental and theoretical studies of the explosion of adiabatically compressed charges. The experimental measurements were carried out in a constant volume spherical combustion bomb previously used to study laminar burning speeds[17]. The fuels studied ranged from butane to octane. Both nitrogen and argon were used as the diluent gas.

A chemical kinetic model based on a chain branch mechanism was developed to simulate both single- and two-stage ignition. For the low temperature, high pressure single-stage process, an analytic solution has been developed[8]. For the high temperature, two-stage process, a kinetic model involving 13 active species and 18 reactions has been developed. The simulated results are in good agreement with experimental data from both the constant volume bomb and rapid compression machines[5,6] if the explosion is assumed to occur in the adiabatic core gas.

EXPERIMENTAL APPARATUS

The spherical combustion bomb used to measure the explosion limits is shown in Fig. 1. The bomb was assembled from flanged 450 alloy steel halves fastened by 6 clamp bolts and sealed by a Viton O-ring. It had an inside diameter of 153 mm and a 19 mm wall thickness, and was designed to withstand pressures up to 1000 atm. Nickel plating on all bomb surfaces provided corrosion resistance and a smooth glossy surface.

The bomb was located in a 400 mm × 400 mm × 460 mm glass-wool oven and heated by eight 250 W resistance heaters mounted on the oven wall and by one 1400 W resistance heater wrapped around the flanges of the bomb. All of the heaters were operated by one on/off temperature controller. An oven fan mounted above the bomb assured temperature uniformity of the oven gases. Four iron-constantan thermocouples distributed within the oven were used to measure temperature. The accuracy of an individual measurement was ±1 K and the bomb temperature was uniform within this accuracy.

Mixtures were ignited by two electrode

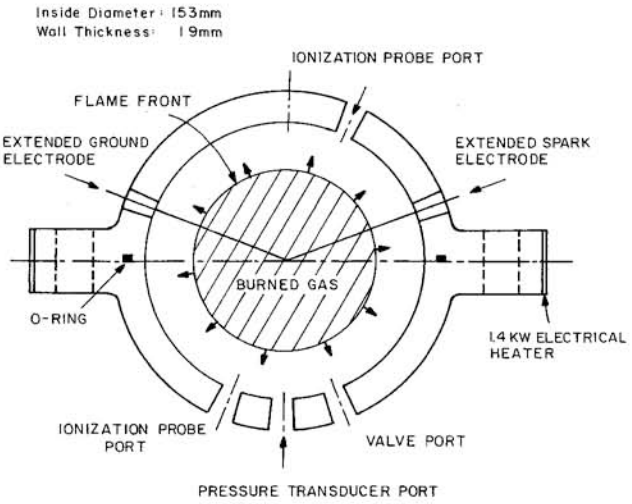

Fig. 1. Schematic diagram of constant volume spherical combustion bomb used to determine explosion limits. In addition to the two ionization gage ports shown, there was a third out-of-plane port (not shown) at the same polar angle as the valve port.

geometries. One was the standard 14 mm DC spark plug; the other had stainless steel electrodes extending to the center of the bomb (Fig. 1). A conventional discharge ignition system with variable voltage and capacitance served to generate the spark.

The gas and fuel handling system is shown in Fig. 2. The liquid fuel handling system was located in the lower temperature fuel oven. Liquid fuel was contained in a stainless steel tube separated from the main manifold and the bomb. A capacitance balance pressure indicator was used to measure the fuel vapor pressure.

Pressures were measured with a Kistler Model 621B piezoelectric pressure transducer. Chemi-ionization associated with either a flame front or an explosion was measured by ionization probes mounted flush with the wall

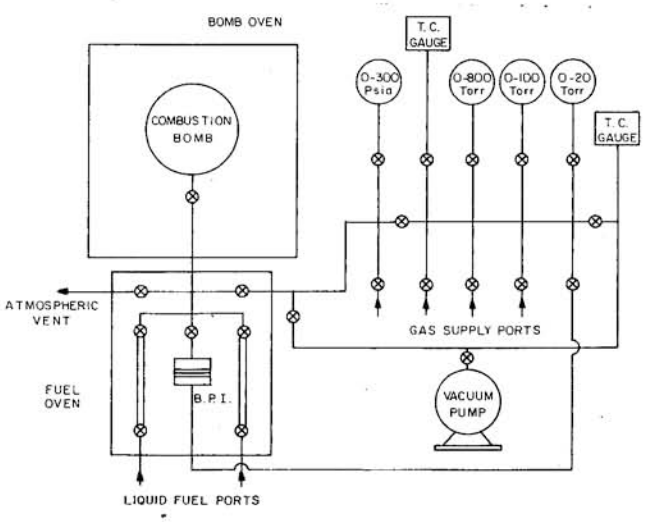

Fig. 2. Gas and fuel handling system for the explosion limit measurements.

at three different locations. Data were recorded using both an oscilloscope and a computer equipped with an A/D converter.

EXPERIMENTAL PROCEDURE

The initial conditions of the combustible charges in the constant volume bomb are critical to insuring the experimental results reliable and repeatable. The state of the combustible mixture just before ignition should be quiescent and homogeneous in temperature and species concentration. The details of the filling procedure are discussed in Ref[19]. The following steps were performed for making a run:

1) evacuate the bomb to a pressure lower than 30 millitorr;

2) feed the fuel vapor into the bomb; monitor the fuel vapor pressure with the Balanced Pressure Indicator;

3) evacuate the manifold; add oxygen to the bomb;

4) evacuate the manifold again; add the diluent gas.

5) wait for five minutes to ensure the gas in the bomb has come to rest and become uniform in temperature and species concentration;

6) fire the bomb; photograph the pressure and ionization traces with the oscilloscope camera; store the pressure data in the computer for later analysis; and,

7) vent the combustion products to the atmosphere.

Typical oscillograms of pressure vs time are shown in Fig. 3 for the combustion of stoichiometric hexane/air mixtures ignited at the center of the bomb at an initial temperature of 473 K. The top oscillogram shows laminar flame development at an initial pressure of 3.2 atm. Compressed by the growing laminar flame front, the pressure of the unburned mixture increases smoothly until it encounters the wall where it goes through a maximum and then decays slowly due to heat loss from the burned gas to the wall. The ionization probe signals show a spread in the arrival times of different parts of flame front at the wall of approximately 0.5 ms. This is typical and indicates spherical symmetry of the flame front to better than one percent. Autoignition of the unburned mixtures with an audible sound was observed during tests having initial pressures higher than 8.0 atm. As shown in the lower two oscillograms, the pressure and ionization probe traces exhibit discontinuities under these conditions. The discontinuities are simultaneous to the accuracy with which they can be read which was approximately ±0.1 ms at the 5ms/cm sweep speed normally used.

A higher speed pressure record is shown in Fig. 4 where it can be seen that the main pressure jump is preceded by a smaller pressure jump occurring approximately 0.2 ms earlier. These pressure traces are qualitatively similar to those observed for rapid compression machines[5,6] and spark ignition engines operating under knocking conditions, and the time interval between the small initial jump and the main pressure jump is interpreted as the second-stage ignition delay.

The explosion pressure was defined as the pressure where the discontinuity occurred on a 5 ms/cm sweep and was reproducible to the accuracy with which the oscillogram could be read. The corresponding explosion temperature was determined from the measured explosion pressure assuming isentropic compression of the unburned adiabatic core gas from the measured initial temperature and pressure. It should be noted that the determination of the explosion pressure by this method is independent of heat losses from the gas as long as the boundary layers are thin and an adiabatic core exists.

To check on the possible effects of the heat transfer and pre-reaction during the settling time, a series of runs were made for each fuel at a fixed initial conditions and various waiting times from 2 min to 10 min. Typical results for stoichiometric butane/O_2/argon and heptane/O_2/argon mixtures are shown in Fig. 5. For settling times greater than two minutes there was no significant dependence of the explosion pressure on the settling time, indicating that steady state initial condition had been reached and pre-reactions were unimportant for the test condition used. Settling times of sive minutes were used for data collection.

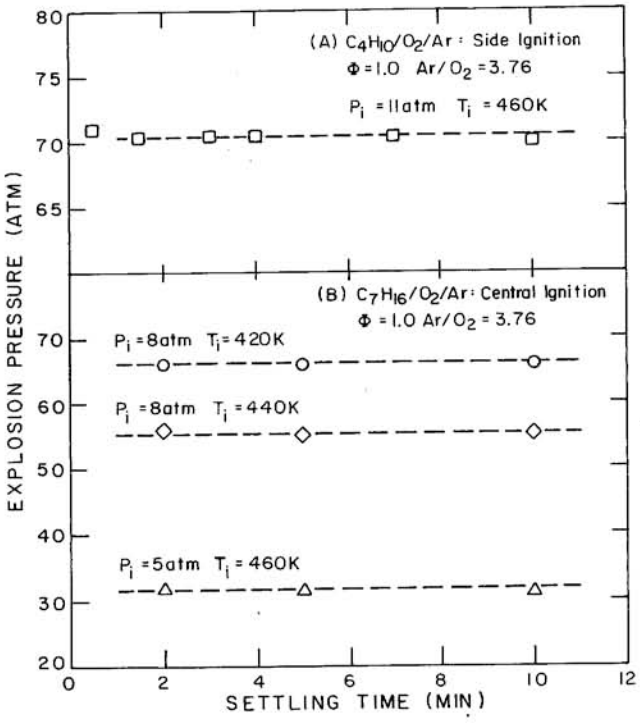

Fig. 5. Explosion pressure as a function of settling time for stoichiometric fuel/O_2/argon mixtures.

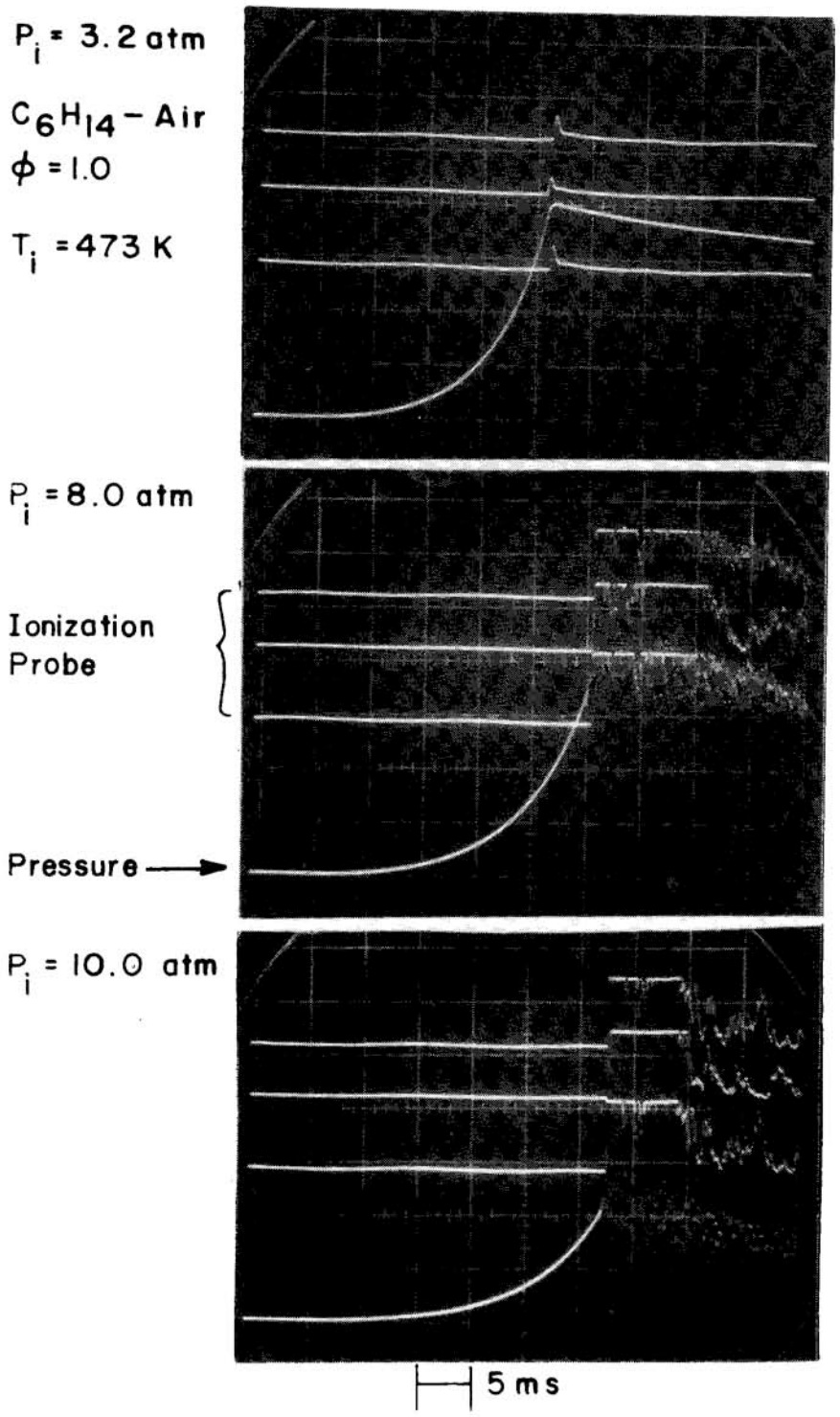

Fig. 3. Normal oscillograms showing pressure and ionization current traces for various initial pressures. The upper record is a typical normal burning process; the two lower records show the typical explosion of end gas prior to completion of normal burning.

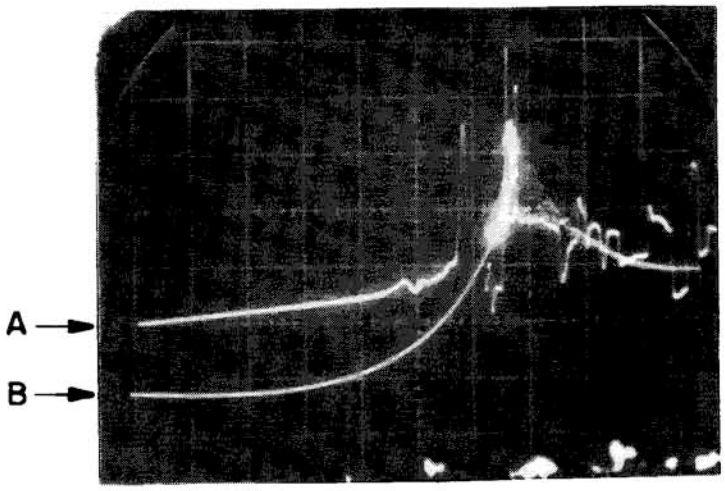

FUEL:	HEXANE + AIR
INITIAL PRESSURE:	8.0 atm
T_i:	465 K
ϕ:	1.0
Horizontal scale:	
A:	5 ms/Div
B:	0.2 ms/Div
Vertical scale:	9.1 atm/Div

Fig. 4. Fast sweep oscillogram of pressure vs time. Trace B shows the high-lighted portion of trace A. The arrows labelled First and Second refer to jumps in trace B associated with the termination of the first and second stage oxidation processes.

EXPERIMENTAL RESULTS

The experimental results for all fuel/oxygen/diluent mixtures studied are shown in Figs 6-10. The initial conditions for each data set are given on the figures. p_i is the initial pressure of the charge in atmospheres; T_i is the initial temperature in K; ϕ is the fuel/air equivalence ratio; and V_o = 22,400 cm^3/mole is the standard molar volume. The oxygen concentration, $[O_2]$, and the temperature, T, at the explosion limit were both calculated from the measured pressure, p, at the explosion limit assuming isentropic compression of the unburned charge from the initial conditions. The estimated accuracy of the pressure measurements was ±3% and the estimated accuracy of the temperature at the explosion limit was ±5 K.

Fig. 6 shows the effect of molecular weight on the explosion limit for normal-alkane/air mixtures. It can be seen that the explosion limit decreases strongly with increasing chain length from butane to octane. Fig. 7 shows the dependence of the explosion temperature on the fuel/air equivalence ratio for normal pentane, hexane and heptane at fixed initial conditions.

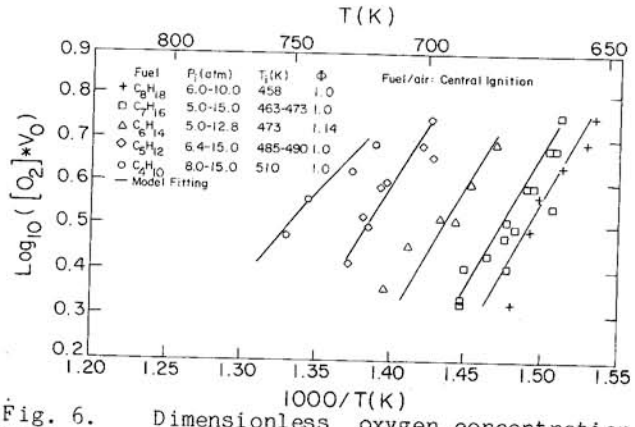

Fig. 6. Dimensionless oxygen concentration $[O_2]V_0$ at the explosion limits as a function of the reciprocal adiabatic core temperature of the unburned gas, 1000/T, for normal alkanes. Curves are fits of model to data using parameters in Tables I and II.

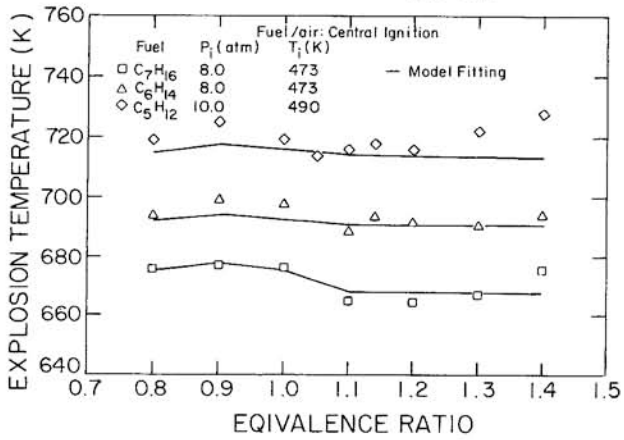

Fig. 7. Explosion temperature as a function of fuel/air equivalence ratio for several fuel at fixed initial temperature. Curves show the model predictions based on data in Tables I and II.

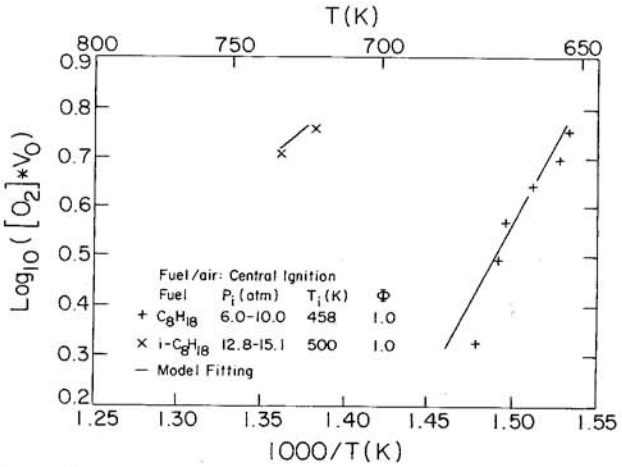

Fig. 8. Dimensionless oxygen concentration, $[O_2]V_0$, at the explosion limits as a function of reciprocal temperature 1000/T, for normal and iso-octane showing the effect of molecular structure. Curves show model fitting using parameters in Tables I and II.

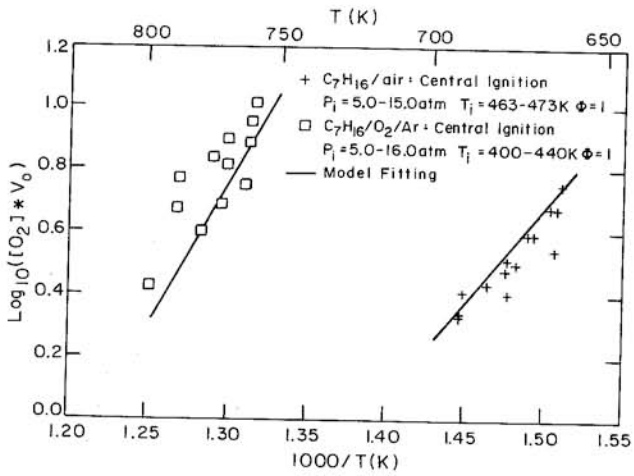

Fig. 9. Dimensionless oxygen concentration, $[O_2]V_0$, at the explosion limits as a function of reciprocal temperature, 1000/T, for heptane showing the effect of the diluent gas. Curves show model fits using parameters in Tables I and II.

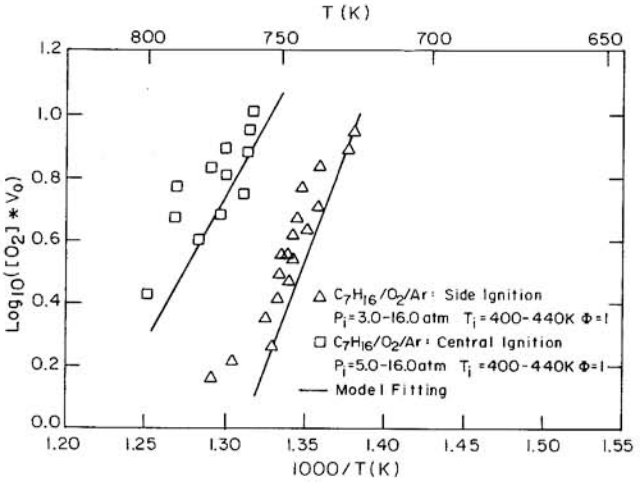

Fig. 10. Dimensionless oxygen concentration $[O_2]V_0$, at the explosion limits as a function of reciprocal temperature, 1000/T, for heptane showing effect of ignition site. Curves show model fits using parameters in Tables I and II.

Over the range 0.8 to 1.4 studied, the explosion temperature is virtually independent of equivalence ratio. Fig. 8 shows the strong effect of molecular structure on the explosion limits for normal and iso-octane/air mixtures. Fig. 9 shows the effect of changing the inert diluent gas from nitrogen to argon for stoichiometric heptane/oxygen mixtures. Finally Fig. 10 shows the effect of moving the ignition site from the center to the side wall of the bomb.

All of the trends in Figs 6-8 are in good qualitative agreement with previous results from engines and rapid compression machines [3,4]. The shift in the explosion limit in Fig. 9 is due primarily to the increase in the adiabatic core temperature and the burning

speed of the unburned gas caused by substituting argon for the nitrogen in the air. The shift in the explosion limit in Fig. 10 is due primarily to the different pressure-time history of the unburned gas associated with the changes in flame geometry and heat loss caused by changing the ignition site.

CHEMICAL KINETIC MODEL

The elementary reactions involved in the oxidation of hydrocarbons have been the subject of numerous investigations over the past fifty years, and many kinetic models for describing the homogeneous explosion of hydrocarbon/oxygen/diluent mixtures have been developed [2,10,11,14,15,21]. It is extremely difficult to track all the reactions and chemical species in the oxidation of hydrocarbons, and most of the chemical rate constants for the reactions are unknown. Thus, it is necessary to use reduced reaction mechanisms to simulate the complicated chemical process. The chemical kinetic model developed in this study is based on the work of Benson[15] and is similar to that of Cox and Cole[11]. It has 13 active species and 18 chemical reactions listed in Table I. It contains four fundamental steps of thermokinetic development: 1) chain initiation; 2) chain propagation; 3) chain branching; and, 4) chain termination. The reactions chosen for this study are not intended to portray all of the chemistry that is possible. Rather they represent a reduced kinetic scheme based on current knowledge.

Reaction is assumed to be initiated by abstraction of a hydrogen atom from the saturated hydrocarbon to yield an alkyl radical and a hydroperoxy radical:

$$RH + O_2 \rightarrow \dot{R} + \dot{H}O_2 \qquad (R1)$$

The alkylperoxy radical isomerization theory[2] was used for the oxidation of alkanes of carbon number greater than four. The main chain cycle involves the following sequence of reactions:

$$\dot{R} + O_2 \leftrightarrow \dot{R}O_2 \qquad (R2)$$

$$\dot{R}O_2 \leftrightarrow \dot{Q}OOH \qquad (R3)$$

$$\dot{Q}OOH + O_2 \leftrightarrow \dot{O}_2QOOH \qquad (R4)$$

$$\dot{O}_2QOOH \rightarrow \dot{O}H + OOQOOH \qquad (R5)$$

$$\dot{O}H + RH \rightarrow \dot{R} + H_2O \qquad (R6)$$

The oxidation of alkyl radicals is by oxygen addition to form the alkylperoxy radical, which then undergoes homogeneous intramolecular rearrangement. Further oxidation of hydroperoxyalkyl radicals by addition of oxygen produces the $\dot{O}_2$ROOH radical. The decomposition of the $\dot{O}_2$ROOH radical usually leads to a hydroxyl radical $\dot{O}H$ and hydroperoxide OROOH. The chain-cycle is then completed by the reaction of the $\dot{O}H$ radical with a fuel molecule. The branching reaction at is assumed to be

$$OROOH \rightarrow \dot{O}H + OR\dot{O} \qquad (R7)$$

Reactions (R1)-(R7) are the principal steps believed to be responsible for oxidation of normal alkanes with carbon numbers greater than 4 at low temperatures, $T < 800$ K, and high oxygen concentrations, $[O_2]V_o > 1$. A reduced kinetic model to simulate the autoignition process in this region has been previously reported[8].

In the high temperature regime ($T > 800$ K, $[O_2]V_o < 1$) hydrogen peroxide, HOOH, replaces hydroperoxide, as the branching agent, and the rapid decomposition of HOOH produces $\dot{O}H$ radicals which accelerate the reaction process. The reaction sequence is

$$\dot{R} + O_2 \rightarrow C{=}C + \dot{H}O_2 \qquad (R8)$$

$$\dot{H}O_2 + \dot{H}O_2 \rightarrow HOOH + O_2 \qquad (R9)$$

$$HOOH + M \rightarrow 2\dot{O}H + M \qquad (R10)$$

Reactions (R1)-(R10) are the principal reactions responsible for the two stage ignition characteristic. A schematic representation of this basic 10 reaction model is shown in Fig. 11. The additional reactions (R11)-(R18) which have been a focus of attention in some models [10,11] were found to be relatively unimportant in the present investigation. In general their effect was small compared to that produced by uncertainties in the rates constants for the primary reactions (R1)-(R10).

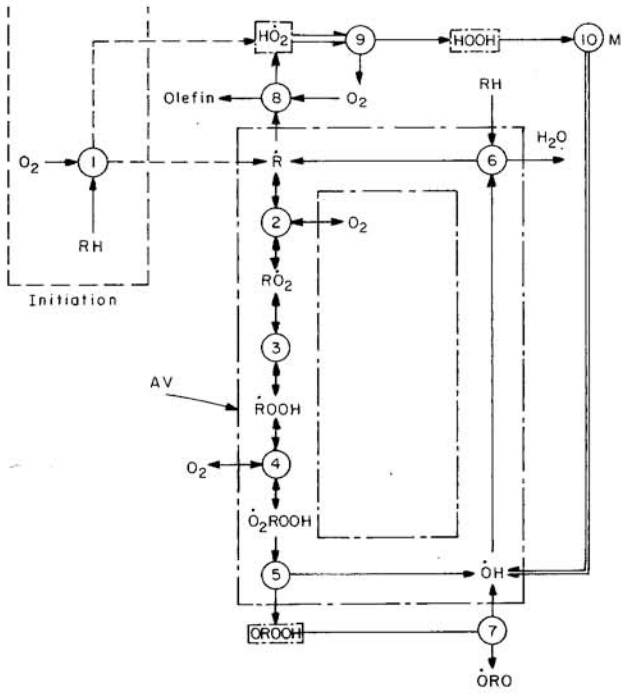

Fig. 11. Schematic of basic 10 reaction model.

NUMERICAL INTEGRATION OF RATE EQUATIONS - The 13 phenomenological rate equations for the species listed in Table 1A were integrated in conjunction with the energy equation using the Gear Method[18]. The rate equations were written in the form

$$\frac{1}{v}\frac{d}{dt}[X_j]v = \sum_{i=1}^{n} (\nu_{ji}^{-} - \nu_{ji}^{+})(R_i^{+} - R_i^{-}) \quad (1)$$

and the energy equation in the form

$$c_p \frac{dT}{dt} = v\frac{dp}{dt} + \sum_{i=1}^{m} (-\Delta H_i)(R_i^{+} - R_i^{-}) \quad (2)$$

where v is the specific volume, ν_{ji}^{-} are the stoichiometric coefficients for species j in reaction i, c_p is the constant pressure specific heat, ΔH_i is the enthalpy change for reaction i, n is the number of reactions, m is the number of species and the forward and reverse reaction rates per unit volume R_i^{+} and R_i^{-} are given by

$$R_i^{\pm} = k_i^{\pm} \prod_{j=1}^{m} [X_j]^{\nu_{ji}^{\pm}} \quad (3)$$

The forward reaction rate constants were expressed in the Arrhenius form

$$k_i^{+} = A_i^{+} \exp(-E_i^{+}/RT) \quad (4)$$

where A_i^{+} and E_i^{+} are constants given in Table 1B and R is the Universal Gas Constant. The reverse rate constants were obtained from the rate quotient law

$$k_i^{-} = k_i^{+} \cdot / K_i \quad (5)$$

where K_i is the equilibrium constant based on concentration for reaction i calculated from thermodynamics data in Ref. 15 and the JANAF Tables. The ideal gas equation of state

$$pv = \left(\frac{\gamma-1}{\gamma}\right) c_p T, \quad (6)$$

where γ is the specie heat ratio, was also used.

COMPARISON OF EXPERIMENT AND THEORY

The chemical kinetic model described in the preceding section was used to calculate explosion limits measured in the constant volume bomb, as well as ignition delay times previously measured in the Thornton and M.I.T. rapid compression machines [5,6].

BOMB EXPLOSION LIMITS - To calculate the explosion limits for the constant volume bomb, it was assumed that prior to an explosion the second term on the right side of Eq (2) representing the sensible energy release rate due to chemical reactions was negligible. The temperature and density were then calculated from the measured pressure curves for normal burning using only the first term on the right side of Eq. (2) and the ideal gas equation (6). Finally the set of rate equations (1) was integrated and the results used to evaluate the neglected sensible energy release rate. The explosion limit was assumed to be reached when the sensible energy release rate became comparable to the first term on the right side of Eq. (2). Due to the exponential increase in the rate of sensible energy release, only the order of magnitude of this term was required to determine the explosion limit with acceptable accuracy.

The explosion limits for heptane obtained using the rate parameters given in Table 1B are compared to the experimental data in Figs 6,7,9 and 10. Considering the sensitivity of the comparison to the exact determination of the temperature and the range of conditions covered by the data, the agreement is remarkably good.

To fit the data for the other fuels studied it is necessary to take into account the effect of molecular weight and structure on the reaction rates. An examination of the kinetic model indicates that the only important reaction expected to be strongly affected by fuel molecular weight and structure is the isomerization reaction (R3) which is in quasistatic equilibrium. In principle the equilibrium constant for this reaction can be determined theoretically from a knowledge of the fuel structure and bond energies. However, such a calculation is difficult and beyond the scope of this paper. The equilibrium constant was therefore represented in the Arrhenius form

$$K_3 = A_3 \exp(-E_3/RT) \quad (7)$$

and the parameters A_3 and E_3 adjusted for each fuel to give the best fit with the data in Figs 6-10. As can be seen the fits obtained were again remarkably good and the parameters obtained are summarized in Table II along with the parameters for heptane obtained from Table IB. For normal alkanes the values of A_3 increase and the values of E_3 decrease with increasing molecular weight. This is in good agreement with expectations based on the number of primary and secondary hydrogen atoms in the molecules. The differences in the parameters for normal- and iso-octane are also in qualitative agreement with expectations based on the number and location of primary, secondary and tertiary hydrogen atoms in these two isomers. Obviously an apriori calculation of the equilibrium constant for reaction (R3) is of considerable interest and much to be desired.

RCM IGNITION DELAYS - Further tests of chemical kinetic model were made by using it

TABLE I
CHEMICAL KINETIC MODEL

A. 13 Active Species

1. RH	2. O_2	3. $\dot{R}$	4. $\dot{RO}_2$	5. ROOH
6. OOROOH	7. $\dot{ORO}$	8. $\dot{OH}$	9. $\dot{HO}_2$	10. HOOH
11. OROOH	12. R'CHO	13. C = C		

B. 18 Reactions (Units: cc, mole, sec, kcal)
Arrhenius parameters of equilibrium constant $K = A\ e^{-E/RT}$ and rate constants $k^{\pm} = A^{\pm}\ e^{-E^{\pm}/RT}$ are for heptane oxidation at 600K < T < 1100K

	Reaction	ΔH_{300}^{o}	log A	E	log A^+	E^+	log A^-	E^-	Refs
1	$RH+O_2 \leftrightarrow \dot{R}+\dot{HO}_2$	46.4	1.5	46.0	13.5	46.0	12.0	0	[15]
2	$\dot{R}+O_2 \leftrightarrow \dot{RO}_2$	-31.0	-1.4	-27.4	12.0	0.0	13.4	27.4	[15]
3	$\dot{RO}_2 \leftrightarrow$ ROOH	7.5	0.9	8.0	11.9	19.0	11.0	11.0	[16]
4	$ROOH+O_2 \leftrightarrow \dot{O}_2RO_2H$	-31.0	-1.9	-27.4	11.5	0.0	13.4	27.4	[8]
5	$\dot{O}_2RO_2H \rightarrow$ OROOH+$\dot{OH}$	-26.6			11.3	17.0			[16]
6	$RH+\dot{OH} \rightarrow \dot{R}+H_2O$	-23.5			13.3	3.0			[23]
7	$OROOH \rightarrow \dot{OH}+\dot{ORO}$	43.6			15.6	43.0			[15]
8	$\dot{R}+O_2 \leftrightarrow \dot{HO}_2$+C=C	-13.5	0.0	-13.5	11.5	6.0	11.5	19.5	[15]
9	$\dot{HO}_2+\dot{HO}_2 \rightarrow HOOH+O_2$	-38.5			12.3	0.0			[15]
10	$HOOH+M \rightarrow 2\dot{OH}+M$	51.4			17.1	46.0			[21]
11	$\dot{ORO} \rightarrow$ R'CHO+$\dot{R}$"	8.5			14.0	15.0			[15]
12	$\dot{ROOH} \rightarrow \dot{OH}$+R'CHO+C=C	-3.0			14.4	31.0			[15]
13	$\dot{RO}_2$+R'CHO $\rightarrow$ ROOH+$\dot{R}$'CO	-0.6			11.45	8.6			[15]
14	$\dot{HO}_2$+R'CHO $\rightarrow$ HOOH+$\dot{R}$'CO	-0.6			11.7	8.64			[15]
15	C=C+$\dot{HO}_2 \rightarrow$ Epox+$\dot{OH}$	-0.23			10.95	10.0			[15]
16	$\dot{HO}_2+RH \leftrightarrow \dot{R}+HOOH$	8.0	0.9	8.0	11.7	16.0	10.8	8.0	[22]
17	$\dot{RO}_2+RH \leftrightarrow \dot{R}+ROOH$	8.0	1.1	8.0	11.2	16.0	10.1	8.0	[15]
18	$\dot{R}+\dot{R} \rightarrow RH$	-85.0			13.2	0.0			[15]

Note: ROOH and OROOH are treated as identical; $\dot{R}$", R'CO and Epox are assumed inactive.

TABLE II

CONSTANTS FOR EQUILIBRIUM CONSTANT OF REACTION 3: $R\dot{O}O \leftrightarrow \dot{R}OOH$

Fuel	log A_3	E_3
Butane	0.0	10.5
Pentane	0.2	8.8
Hexane	0.6	8.5
Heptane	0.9	8.0
Octane	1.1	8.0
Iso-octane	0.0	11.4

to predict the two-stage ignition process obtained in the Thornton rapid compression machine. In the published analysis of this work[6], the authors used the mean gas temperature determined from the ideal gas equation of state to correlate their data. Because of relatively large heat losses in the Thornton machine, this temperature is significantly lower than the expected adiabatic core gas temperature. Using original data, kindly supplied by the authors, we have calculated the adiabatic core temperature and used them to reanalyze the Thornton results for iso-octane.

Examples of the simulated temperature vs time profiles are shown in Fig. 12 both for the full 18 reaction model and the basic model including only the first 10 reactions in Table IB. It can be seen that the well documented two-stage ignition process is reproduced by both models and that the difference between them is relatively small involving primarily the second-stage ignition delay time τ_2.

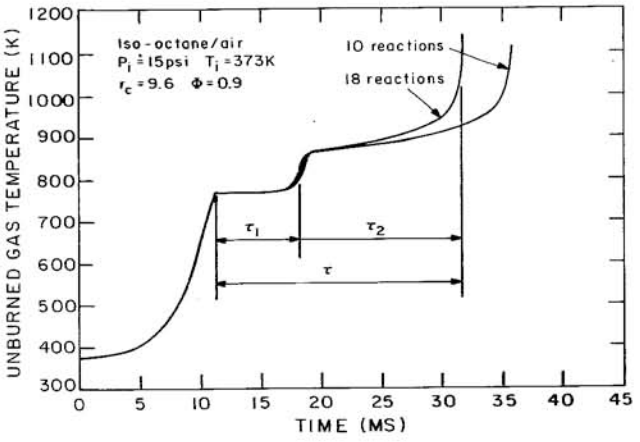

Fig. 12. Calculated temperature-time histories for a rapid compression machine showing typical two stage ignition process. Curves show effect of different modeling assumption on the duration of the two stages. Only the second stage is significantly affected by the omission of reactions R11-R18.

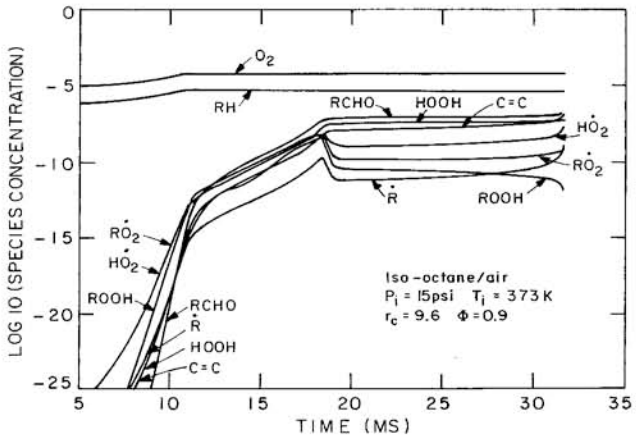

Fig. 13. Simulated concentrations of major species vs time for the 18 reaction model. Rate constants for the reactions are listed in Tables I and II.

The corresponding concentration vs time profiles for the 18 reaction model are shown in Fig. 13. To avoid excessive overlapping of curves only the 9 most abundant species have been included. During the first stage the concentrations rise geometrically to values of order 10^{-12} moles/cm^3 at which point degenerate branching becomes important and the rise becomes exponential. The first stage is terminated when the reaction

$$\dot{H}O_2 + \dot{H}O_2 \rightarrow HOOH + O_2$$

become important at which point the hydroperoxide and radical concentrations decrease and the second stage begins. During the second stage the concentrations of intermediates is steady but the temperature continues to rise until the branching reaction

$$HOOH + M \rightarrow \dot{H}O + \dot{H}O + M$$

becomes important at which point the radical concentration starts to exponentiate again and an "explosion" occurs. Note that contrary to expectations based on prior work[10,11], the aldehyde RCHO plays no significant role in this process, though it undoubtedly becomes important during the explosion itself since it is the precursor to CO formation.

The sensitivity of the temperature-time profiles to two key rate parameters is shown in Figs 14 and 15. Fig. 14 shows the effect of varying the heat of reaction E_3 for reaction (R3) and it can be seen that variations of as little as ±0.5 K cal produce substantial changes in both the first and second stage ignition delay times. Indeed the variations are larger than those shown in Fig. 12 caused by the omission of reactions (R11)-(R18) in the model. Fig. 15 shows the effect of varying log A_{10}^+ by ±0.1. In this case, the first stage ignition delay time is unaffected while the second stage delay time undergoes changes which are again comparable

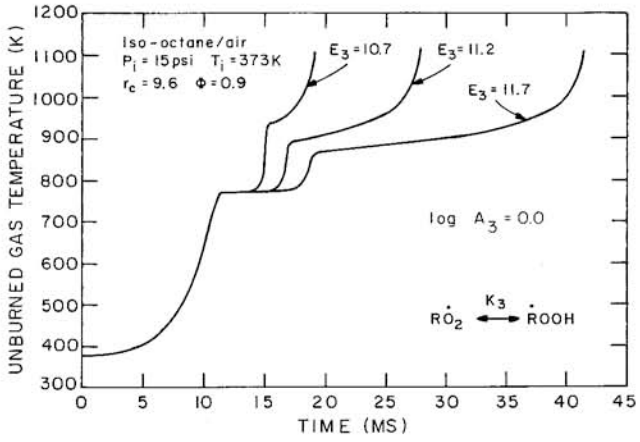

Fig. 14. Effect of varying the rate parameter E_3 on the predicted temperature-time profile for a rapid compressing machine.

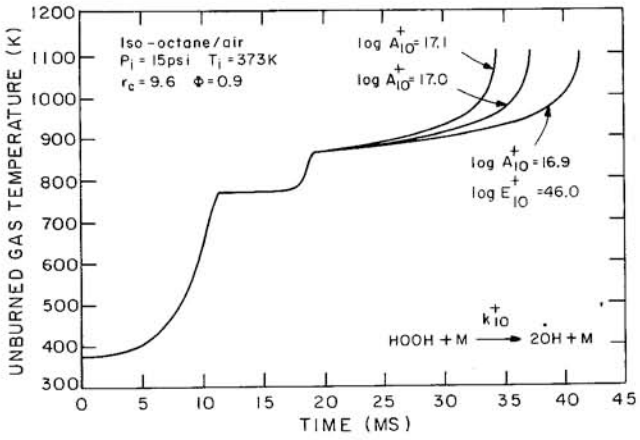

Fig. 15. Effect of varying the rate parameter A_{10}^+ on the predicted temperature-time profiles for a rapid compression machine.

to those caused by the omission of reactions (R11)-(R18) in the model.

The effect of heat loss on the temperature vs time profiles is shown in Fig. 16 where total ignition delay times for several initial pressures are plotted as a function of the reciprocal temperature for both the adiabatic core temperature used in the present analysis and the mean gas temperature used in the analysis of Ref[6]. It can be seen that the two sets of curves are similar in shape but the adiabatic core temperature is approximately 80K higher than the mean gas temperature. On the time scale of the experiments it is unlikely that significant mixing of the cooler boundary layer gases with the adiabatic core gas occurs and since reaction will proceed most rapidly in the highest temperature zone, it is the adiabatic core temperature which would be expected to control the ignition delays. It should also be noted that using the adiabatic core temperature resolves the disagreement between the experimental results reported in Ref[5] and Ref[6].

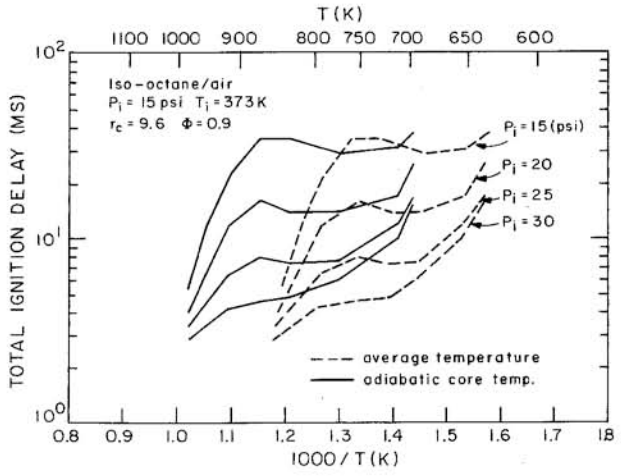

Fig. 16. Calculated total ignition delay times plotted as a function of average and adiabatic unburned gas temperatures for the Thornton RCM for several initial pressures. Rate parameters were taken from Tables I and II.

A comparison of the Thornton experimental data[6] with the model prediction is shown in Fig. (17) where the total ignition delay time is plotted as a function of the reciprocal adiabatic core temperature for several initial pressures. The rate constants used in the model are those given in Tables I and II. Considering the uncertainty in both the experimentally measured temperatures and the rate constants used in the model the agreement is remarkably good. Unlike previous analyses[6,11], only minor adjustments in the previously published rate constants were required.

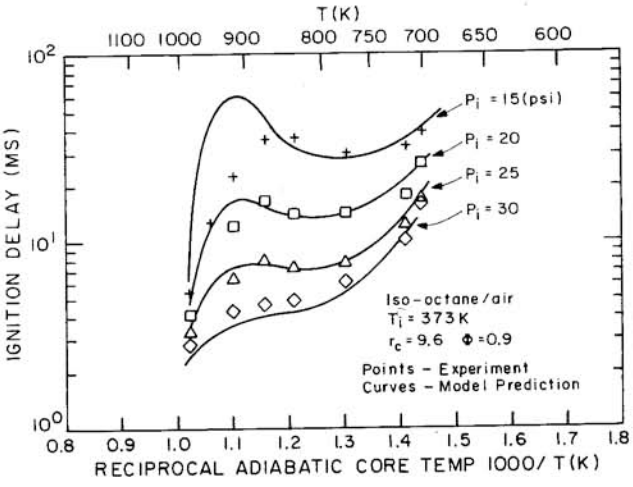

Fig. 17. Comparison of total ignition delay times measured in the Thornton RCM with model predictions for several initial pressures. Rate parameters were taken from Tables I and II.

Further comparisons between experiment and theory are shown in Fig. (18) in which the various ignition delay times are plotted as a function of initial pressure for fixed initial temperature. Once again the agreement is good.

A comparison between the experimental data from M.I.T. rapid compression machine[5] with theory is shown In Fig. (19). In these experiments, the initial temperature, pressure and mixture composition, were fixed and the compression ratio was varied. Good agreement has been achieved between the experimental data and the model prediction by using the parameters listed in Table I and II.

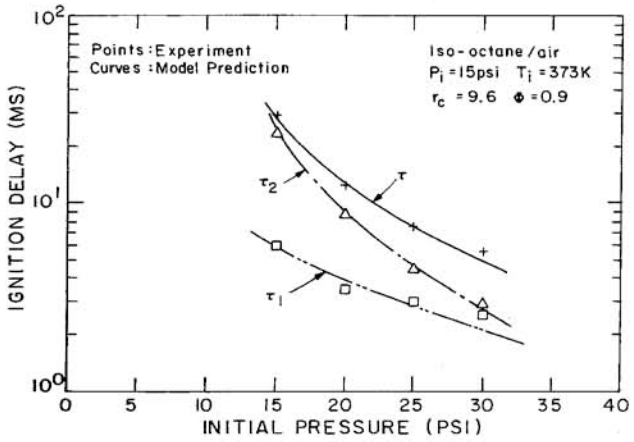

Fig. 18. Comparison of various delay times measured in the Thornton RCM with model prediction for an 0.9 stoichiometric iso-octane/oxygen/diluent mixture. Curves represent modeling results using parameters in Table I and II and the symbols represent experimental data.

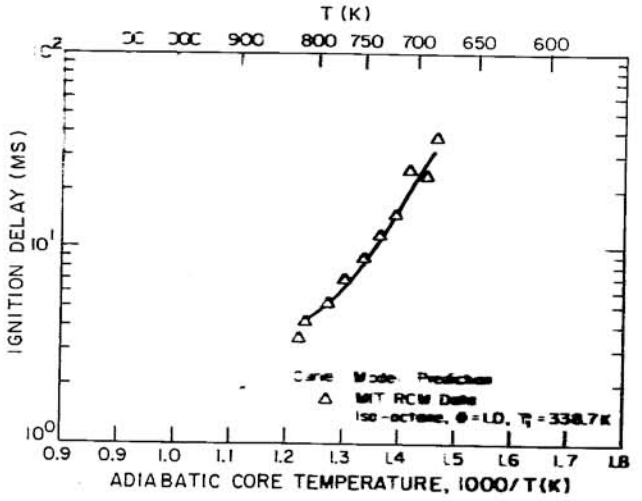

Fig. 19. Comparison of MIT RCM experimental data with model predictions for a stoichiometric iso-octane/air mixture. Curve represents modeling results using parameters in Table I and II and the symbols represent experimental data.

SUMMARY AND CONCLUSIONS

Measurements of the explosion limits for homogeneous hydrocarbon/oxygen/diluent mixtures compressed adiabatically by a spherical flame front have been made in a constant volume spherical combustion bomb under well defined conditions. A chemical kinetic model which contains 18 chemical reactions and 13 active species, has been developed to simulate the autoignition process. Comparisons between the experimental data and simulated results are in good agreement.

On the basis of this work, the following conclusions can be drawn:

1) The constant volume spherical bomb is a useful facility for the investigation of auto-ignition in adiabatically compressed gas mixtures under controlled conditions.

2) A relative simple branched chain kinetic model can be used to describe the two-stage ignition process in constant volume bombs and rapid compression machines.

3) Hydroperoxide is the important branching agent in the first stage and hydrogen peroxide is the important branching agent in the second stage.

4) The first stage is terminated by the reaction $\dot{HO}_2 + \dot{HO}_2 \rightarrow H_2O_2 + O_2$ and an explosion occurs when the reaction $H_2O_2 + M \rightarrow 2\dot{O}H + M$ becomes important.

5) The effects of fuel molecular weight and structure are related to the equilibrium constant for the reaction $R\dot{O}O \rightarrow ROOH$.

6) The adiabatic core temperature controls the auto-iginition process and should be used for correlating experiment and theory.

7) Comparison of constant volume bomb and rapid compression machine data shows no observable effects due to compression by a hot flame front rather than a cold piston.

ACKNOWLEDGEMENTS

The authors would like to thank Dr. L.J. Kirsch for supplying original data from the Thornton Rapid Compression Machine experiments.

This work was supported by the U. S. Department of Energy, Office of Energy Utilization Research, Energy Conversion and Utilization Technologies Program.

REFERENCES

[1] Lewis, B. and von Eble, G, "Combustion, Flames and Explosion of Gases," Academic Press, New York, 1961.

[2] Pollard, R.T., "Comprehensive Chemical Kinetics," Volume 17, C.H. Bamford and C.F.H. Tipper, Eds., Elsevier, Amsterdam(1977).

[3] Taylor, C.F. and Taylor, E.S., "The Internal Combustion Engine," International Textbook Co., Scranton, PA 1966.

[4] Obert, E.F., "Internal Combustion Engines and Air Pollution," Intext Educational Publisher, New York, (1973).

[5] Taylor, C.F., Taylor, E.S., Livengood, J.C., Russell, W.A., Leary,W.A., " Ignition of Fuels by Rapid Compression," SAE Quarterly Transaction, Volume 4, No. 2, pp.232, (1950).

[6] Halstead, M.P., Kirsch, L.J. and Quinn, C.P., "The Autoignition of Hydrocarbon Fuels at High Temperatures and Pressures-Fitting of a of a Mathematical Model," Combustion and Flame, Volume 30, pp.45, (1977).

[7] Livengood, J.C. and Wu, P.C.,"Correlation of Autoignition Phenomenon in Internal Combustion Engines and Rapid Compression Machines," 5th International Combustion Symposium, pp.34, The Combustion Institute (1955).

[8] Keck, J.C. and Hu. H., "Explosion of Adiabatically Compressed Gases in a Constant Volume Bomb," 21st Symposium(international) on Combustion, Munich, West Germany, (1986).

[9] Pitz, W.J. and Westbrook, C.K., " Chemical Kinetics of the High Pressure Oxidation of n-Butane and Its Relation to Engine Knock,"Combustion and Flame 63, pp.113, (1986).

[10] Halstead, M.P., Kirsch, L.J., Prothero, A. and Quinn, C.P., " A Mathematical Model for Hydrocarbon Autoignition at High Pressure," Proc. Roy. Soc., A346, pp.515, (1975).

[11] Cox, R.A. and Cole, J.A.,"Chemical Aspects of the Autoignition of Hydrocarbon/ Mixtures," Combustion and Flame 60, pp.109, (1985).

[12] Schapertons, H. and Lee, W., "Multi-dimensional Modelling of Knock Combustion in SI Engines," SAE 850502 (1985)

[13] Theobald, M.A. and Cheng, W.K.," A Numerical Study of Diesel Ignition," ASME Paper, 87-FE-2, (1987).

[14] Trumpy, D.K., Uyehara, O.A. and Myers, P.S.,"The Preknock Kinetics of Ethane in a Spark Ignition Engine," SAE Trans SAE 690518, (1969).

[15] Benson, S.W., "The Kinetics and Thermochemistry of Chemical Oxidation With Application to Combustion and Flame," Prog. Energy Combust. Sci. Vol. 7, pp.125, (1981), see also Oxidation Communication Vol. 2, pp.169, (1982).

[16] Baldwin, R.R., Hiskam, M.W.M., Walker, R.W., "Arrhenius Parameters of Elementary reactions Involved in the Oxidation of Neopentane," J. Chem. Soc., Faraday Trans. 1, 78, pp.1615 (1982).

[17] Metghalchi, M and Keck, J.C., " Burning Velocities of Mixtures of Air with Methanol, Isooctane, and Indolene at High Pressure and Temperature," Combustion and Flame 48, pp.191, (1982).

[18] Hindmarsh, A.C.," Gear: Ordinary Differential Equation System Solver," UCID-30001, (1974).

[19] Hu, H.,"The Autoignition of Hydrocarbon-Oxygen-Diluent Mixtures in a Constant Volume Bomb," Sc. D. Thesis, M.I.T., (1987).

[20] Lightfoot, N.S. and Negus, C.R., 20th International Symposium on Combustion, pp.111, The Combustion Institute (1984).

[21] Baulch, D.L., Drysdal, D.D., Duxbury, J. and Grant, S., "Evaluated Kinetic Data for High Temperature Reactions," pp.3, Butterworths, London, (1976).

[22] Sahetchian, K.A., Heiss, A., Rigny, R. and Ben-Aim, R.I., "Determination of the Gas-Phase Decomposition Rate Constants of Heptyl-1 and Heptyl-2 Hydroperoxides $C_7H_{15}OOH$," Int. J. Chem. Kinet. 14, pp.1325 (1982).

[23] Cohen, N. and Westburg, K.R., Aerospace Report No. ATR-82(7888)-3 (1982).

[24] Morgan, C.A., Pilling, M.J. and Tullock, J.M., "Direct Determination of the Equilibrium Constant and Thermodynamic Parameters for the Reaction $C_3H_5 + O_2 \leftrightarrow C_3H_5O_2$," J. Chem. Soc., Faraday Trans. 2, 78, pp.1323 (1982).